PAPER

Theoretical insight into effect of doping of transition metal M (M = Ni, Pd and Pt) on CO_2 reduction pathways on Cu(111) and understanding of origin of electrocatalytic activity†

Lihui Ou,*[ab] Wenqi Long,[a] Jianxing Huang,[a] Yuandao Chen[ab] and Junling Jin[a]

The effect of the doped transition metal M (M = Ni, Pd and Pt) on CO_2 reduction pathways and the origin of the electrocatalytic activity are investigated systematically by focusing on the CH_4 and CH_3OH formation pathways based on DFT calculations associated with the computational hydrogen electrode model. Our studies show that the doping of Ni, Pd and Pt can promote CO_2 reduction into hydrocarbons and influence the selectivity of reduction pathways, in which the doping of Pt may be able to lead to the strongest catalytic activity. The adsorption behavior between reaction intermediates and surfaces is crucial and the interactions of intermediates with the catalysts should be moderate in order to efficiently catalyze CO_2 reduction into CH_4 and CH_3OH, and avoid OH surface poisoning. The enhanced electrocatalytic activity of transition metal-doped Cu(111) surfaces may be owing to decreased overpotential and moderate electronic interactions between Cu and the doped transition metals. The doped Ni, Pd and Pt atoms can considerably decrease the overpotential and remove surface OH poisoning, in which the doped Pt can simultaneously reduce overpotential for CO formation and further reduction, and most easily remove OH, thus suggesting the best electrocatalytic activity. The moderate electron interaction between Cu and Pt and moderate upshift of the d-band center of Pt also explain why the Pt-doped Cu(111) surface has the best electrocatalytic activity for CO_2 reduction. Two possible descriptors can be proposed in order to scale the electrocatalytic activity of Cu-based electrocatalysts for CO_2 reduction, in which an ideal Cu-based electrocatalyst should be able to reduce barriers for CO formation and further reduction, and should have moderate electron interactions between Cu and the doped transition metals, and a moderate upshift of d-band center of the doped transition metals. In these ways, CO_2 reduction pathways can be facilitated and the yield of hydrocarbons CH_4 and CH_3OH can be enhanced.

1. Introduction

Excessive consumption of fossil fuels has gradually led to the increasing anthropogenic emission of CO_2 and depletion of finite natural resources.[1] To mitigate over-production of CO_2 and prepare for a fluctuating supply of fossil fuels, efforts are being made to convert CO_2 into reusable hydrocarbons.[2] Among various approaches for conversion, electrochemical reduction of CO_2 is considered a potentially clean and promising technique to produce various value-added hydrocarbons at only the cost of a sustainable supply of electrical energy.[3,4] However, the

selectivity and faradic efficiency of the CO_2 electroreduction process are dependent on many factors, such as the electrode materials, the surface structures of the electrode and the type of electrolytes,[5–10] in which the major obstacle preventing the efficient reduction of CO_2 is the lack of electrode materials that can readily couple with electric energy to achieve rapid and selective cleavage of C–O bonds in CO_2 and formation of new bonds in the products. Towards this goal, various electrode materials and promoters have been screened experimentally and analyzed computationally to optimize their activity and selectivity for CO_2 reduction,[10–19] such as transition metals,[15] ionic liquids,[16] organometallic complexes[17,18] and doped graphene.[19] Unfortunately, present electrocatalysts for CO_2 reduction suffer from high overpotentials, low current densities, low selectivity or poor durability.[20] Among these electrocatalysts explored to date, Cu has received considerable attention because it has been demonstrated experimentally as a valid low-cost electrocatalyst for CO_2 reduction[21,22] and is the only pure

[a]College of Chemistry and Materials Engineering, Hunan University of Arts and Science, Changde 415000, China

[b]Hunan Province Cooperative Innovation Center for the Construction & Development of Dongting Lake Ecologic Economic Zone, Hunan University of Arts and Science, Changde 415000, China. E-mail: oulihui666@126.com; Tel: +86-736-7186115

elemental catalyst that produces hydrocarbons at significant faradic efficiency.[20] Reduction products include formate, CH_4, C_2H_4 and other higher hydrocarbons.[23–26] Furthermore, theoretical study of CO_2 reduction on transition metals Cu, Pt, Rh, Pd, Ni, Au and Ag by Nørskov and co-authors[27] revealed the "volcano" type of the activity diagram, in which Cu has also the best catalytic activity and is located at the top of the diagram among these transition metals. Thus, experimental and theoretical studies all showed that Cu is the best known metal electrocatalyst for CO_2 reduction. However, in order to achieve high faradic efficiency, significant overpotentials are required on Cu electrodes. For example, the theoretical reversible potentials for CH_4 and C_2H_4 are 0.17 V and 0.08 V (vs. RHE), respectively, but experimentally it was observed that a very large potential of about −1.0 V is applied for CO_2 reduction into these hydrocarbons.[28] Simultaneously, the H_2 evolution reaction (HER) at sufficiently negative potential can reduce the faradic efficiency for CO_2 reduction by consuming protons and electrons. Thus, to make the CO_2 reduction more active and selective, properly designing new electrocatalysts is extremely urgent under the current situation.

In surface-catalyzed reactions, the surface selectivity, activity and stability can be dramatically improved through the doping of transition metals to the surface of a host, and some novel properties that are not present on the parent metal surfaces are often exhibited.[29–32] Thus, bimetallic Cu-based alloys with Cu-rich composition experimentally have been extensively used to improve CO_2 electroreduction owing to the high overpotential and low current density of the pure Cu surface, such as Cu–Ni, Cu–Zn, Cu–Cd, Cu–Sn, Cu–Pb, Cu–Au, Cu–Ag, Cu–Pd and Cu–Pt.[33–40] Compared to pure Cu, doping of other transition metals into Cu catalysts can modify the activation barrier for different steps, thereby leading to a reduction of overpotential and a major change of faradic efficiency. For example, Cu–Au alloy has higher faradic efficiency for CO_2 electroreduction than that of pure Cu,[37] and the experimental onset potential on the Cu–Au alloy was positively shifted, indicating that the overpotential of CO_2 reduction can be reduced through the doping of Au.[38] The Ni-doped Cu surface also displayed experimentally a superior catalytic activity with respect to the CH_3OH synthesis from a mixture of CO, CO_2 and H_2 in comparison with pure Cu.[39,40] Such an improvement was ascribed to the capability of Ni to promote CH_3OH production by activating CO_2 and stabilizing the intermediates owing to the higher oxygen affinity of Ni.[41] Recently, a Pd–Cu catalyst for CO_2 electroreduction was investigated.[42] A sharp increase of the reduction current and positive shift of potential were observed on the Pd–Cu electrode compared with those for pure Cu, indicating that the doping of Pd could effectively suppress the HER and enhance the CO_2 electroreduction activity. Actually, in more previous studies, both Pd single-crystal[43] and oxide-supported Pd catalysts[44,45] have also been shown to be catalytically active toward CH_3OH synthesis from CO_2 reduction. Given that Pt is also a metal with high chemical stability and oxygen affinity, the doping of Pt could be a promising approach to improve CO_2 electroreduction. Thus, a Cu–Pt alloy with high Cu concentration was developed by Xiong and co-authors. The greatly improved

chemical stability and superior electrocatalytic activity towards CO_2 reduction were exhibited owing to the presence of Pt.[36] Moreover, the alloying of Cu with Pt can lower the decomposition activation energy of formate by up to 13%.[46] In the recent theoretical studies on CO_2 reduction, density functional theory (DFT) was employed by Liu and co-authors to investigate the CH_3OH synthesis reaction from CO_2 reduction on transition metals-doped Cu(111) surfaces.[47] The overall CH_3OH yield was increased by the doped Ni, Pd and Pt compared with pure Cu, suggesting that the doping of Ni, Pd and Pt is able to promote the CH_3OH production of the Cu(111) surface. Using DFT calculations associated with the standard hydrogen electrode model,[48,49] Hirunsit and co-authors performed a systematic thermodynamic investigation for CO_2 electroreduction into CH_4 and CH_3OH on Cu-based electrocatalysts with a Cu-rich composition of Cu_3X (X is Ag, Au, Co, Ni, Pd, Pt, Rh and Ir). The investigation exhibited that a considerably different electrocatalytic activity was produced and hydrocarbon selectivity was changed compared with those on the pure Cu surface, in which on the mostly Cu-based alloy catalysts CH_4 is more energetically favorable to be yielded than CH_3OH, and CH_3OH was found to be more favorable than CH_4 production on Cu_3Pd and Cu_3Pt surfaces. On most surfaces the potential-limiting step is the CO protonation with the exception of on Cu_3Au and Cu_3Co surfaces. Most recently, the activation of CO_2 on transition metal TM (TM = Fe, Co, Ni, Ru, Rh, Pd, Ag, Os, Ir, Pt and Au)-doped Cu(111) and Cu(100) surfaces was investigated with a dopant coverage of 1/9 ML by Qiu and co-authors using first-principle DFT calculations combined with a slab model.[50,51] The studies predicted that Co, Ru and Os may be potential dopants to enhance the chemisorption of CO_2 on both TM-doped Cu surfaces. However, previous experimental and theoretical studies only showed that the doped transition metals could reduce the thermodynamic overpotential of CO_2 reduction and activate CO_2 molecules. The exact CO_2 electroreduction mechanisms and origin of electrocatalytic activation on Cu-based electrocatalysts still remain unclear, especially kinetic analysis of the elementary reaction steps and the relationship between the kinetic barriers and adsorption ability of the reaction intermediates. Essentially, the doping of transition metals can change the CO_2 reduction pathways and reduce the activation barriers, thereby leading to the reduced overpotential and enhanced catalytic activity. A general understanding of the adsorption behavior, reaction mechanism and atomic-level origin of the electrocatalytic activity of Cu-based catalyst bimetallic surfaces will help us discover more efficient catalysts for a given reaction.

Based on the above analysis, Ni, Pd and Pt atoms as potential dopants may be able to enhance CO_2 reduction into hydrocarbons on the Cu surface. Furthermore, Cu, Ni, Pd and Pt have the same face-centered cubic structure, which gives them a crystallographic match. Thus, the activation barriers of key steps can be maneuvered through the miscible bimetallic combinations of Cu with Ni, Pd and Pt, thereby resulting in improved surface catalytic activity and selectivity. Focusing on the CH_4 and CH_3OH formation pathways, the effect of the doped transition metal M (M = Ni, Pd and Pt) on the CO_2 reduction pathways and

the origin of the electrocatalytic activity are investigated systematically based on DFT calculations associated with the computational hydrogen electrode model. The (111) facet is chosen owing to its high selectivity for CH_4 production. The major goal of this work is to examine the effects of the doped Ni, Pd and Pt atoms on the CO_2 reduction pathways, surface electrocatalytic activity and selectivity in comparison with pure Cu catalyst. Some key factors that influence surface electrocatalytic activity, such as OH surface poisoning, the limiting potential, potential-limiting step and electronic interactions between Cu and Ni, Pd and Pt, are also demonstrated. The development of more superior electrocatalysts requires an essential understanding of these effects.

2. Computational method and modeling

All DFT calculations were implemented through the PWSCF codes included in the Quantum ESPRESSO distribution,[52] while figures of the chemical structures were produced by the XCRYSDEN graphical package.[53–55] The exchange–correction interactions were treated by using the generalized gradient approximation (GGA) of Perdew–Burke–Ernzerhof (PBE).[56] The nuclei and core electrons were described by ultrasoft pseudopotentials.[57] The transition metal M (M = Ni, Pd and Pt)-doped Cu electrodes modeled by three-layer (111) slabs with a 2 × 3 supercell were used to perform the calculations of the all stable geometry structure of various adsorption and co-adsorption intermediates, which has been shown to be thick enough to well describe the CO_2 reduction. The calculated equilibrium lattice constant of Cu was 3.66 Å, which was in good agreement with experimental and theoretical values (3.62 and 3.66 Å, respectively).[58,59] During the geometry optimization, the bottom two atomic layers in the transition metal M (M = Ni, Pd and Pt)-doped Cu(111) slabs were kept fixed, whereas the top one layer and the adsorbates were relaxed to geometry configurations with the lowest energy. A vacuum region of 16 Å was used along the z-direction to avoid any periodic interactions. For the 2 × 3 supercell, the surface Brillouin zone was sampled by using a 4 × 3 × 1 uniformly shifted k-mesh. The Kohn–Sham orbitals were expanded in a plane-wave basis set, and the plane-wave cutoff energy was optimized at 26 Ry. The smearing technique of Methfessel and Paxton was used to treat the Fermi-surface effects with a value of smearing parameter of 0.02 Ry.[60] The convergence criteria for the total energy and Cartesian force components acting on each atom were set to within 10^{-5} Ry and below 10^{-3} Ry Bohr^{-1}, respectively. Additionally, it has been shown that dopants Pd and Pt prefer to stay in the surface of Cu(111), while Ni is in favor of the bulk.[61] However, based on the experiments conducted by Chorkendorff and coauthors,[39,40] the active adsorbents are able to pull the Ni atom out to the surface under hydrocarbon synthesis conditions, such as CO. Thus, our present study did not include the segregation of Ni into the bulk. The doping range of dopants on the Cu-based electrocatalyst surfaces from ca. 1/9 to 1/4 has been studied in the previous experimental and theoretical studies,[35,36,47,50,51,62] and

the surface with dopant coverage of ca. 1/6 ML has superior electrocatalytic activity towards CO_2 reduction. Thus, only one surface Cu atom was substituted by a dopant (Ni, Pd and Pt) atom in each periodic supercell in the present study, corresponding to a dopant coverage of 1/6 ML. Selecting dopant coverage of 1/6 ML is also in order to compare with our previous studies on a pure 2 × 3 Cu(111) surface.[63]

The minimum energy paths (MEPs) for each step of the CO_2 reduction into hydrocarbons were determined by the climbing-image nudged elastic band (CI-NEB) method.[64,65] The image of highest energy approximated the transition state of the optimized reaction coordinate, and the transition state images from the CI-NEB calculations were optimized by the quasi-Newton method, which minimizes the forces to find the saddle point. For each intermediate point in the MEPs, geometry optimization was also performed.

3. Results and discussion

3.1 The optimal reaction pathways of CO_2 reduction

The calculated results of CO_2 reduction into CH_4 and CH_3OH on the pure Cu(111) surface were reported in our previous work[63] and are summarized in the ESI† again to complete the systematic comparison. Various possible pathways obtained by minimum energy pathway (MEP) analysis during the course of CO_2 reduction on transition metal M (M = Ni, Pd and Pt)-doped Cu(111) are also demonstrated in the ESI.† Based on the MEP analyses of the elementary reaction steps, it can be concluded that CO, CHO and CH_2O are key reaction intermediates during the course of CO_2 reduction into hydrocarbons on Ni-, Pd- and Pt-doped Cu(111) surfaces, in which CO is firstly formed through CO_2 dissociative hydrogenation, and the COOH intermediate is involved during the course of CO formation. On the Ni-doped Cu(111) surface, formation of intermediates CH_3O, CH_2OH and CH_2 through further CH_2O hydrogenation and hydrogenative dissociation are all favorable reaction pathways, which may be parallel pathways in the CO_2 reduction mechanism based on the MEP analyses. CH_3OH formation more easily occurs through CH_2OH hydrogenation in CH_3O and CH_2OH further reduction on the Ni-doped Cu(111) surface. Simultaneously, CH_2 that is produced through CH_2O hydrogenative dissociation also leads to CH_4 formation. Notably, CH_2OH hydrogenation into CH_3OH formation and CH_2 serial hydrogenation into CH_4 require very low activation barriers on the Ni-doped Cu(111) surface, which can be all overcome by the thermoactive process at ambient temperature. Thus, we conclude that CH_4 and CH_3OH may be able to be formed during CO_2 reduction simultaneously on the Ni-doped Cu(111) surface. The MEP analyses on the Pd-doped Cu(111) surface show that CH_2O direct hydrogenation into CH_3O is the most favorable pathway among all possibilities of further CH_2O reduction. The most preferred reaction pathway among further CH_3O reduction is CH_3O hydrogenative dissociation into CH_3 on the Pd-doped Cu(111) surface. Thus, CH_4 can be formed through CH_3 hydrogenation. On the Pt-doped Cu(111) surface, direct hydrogenation of CH_2O to form CH_3O and CH_2OH intermediates are the most favorable pathways. Thus, CH_3O and CH_2OH may be

reaction intermediates in CO_2 reduction on the Pt-doped Cu(111) surface. The MEP analyses show that CH_3 and CH_3OH can be formed easily through CH_3O hydrogenative dissociation and CH_2OH hydrogenation, respectively. Simultaneously, a CH_2 intermediate can be also formed through CH_2OH hydrogenative dissociation. Intermediates CH_2 serial hydrogenation and CH_3 hydrogenation possibly result in the formation of the final CH_4 product. Thus, we can conclude that CH_4 and CH_3OH in CO_2 reduction on the Pt-doped Cu(111) surface are also possible products. Based on thermodynamic and kinetic analyses, $(CO + H)^* \rightarrow CHO^*$ is the slowest step on these three surfaces. The optimal reaction pathways of CO_2 reduction on the pure and transition metal M (M = Ni, Pd and Pt)-doped Cu(111) surfaces are summarized in Fig. 1.

3.2 Comparison of CO_2 reduction pathways among pure and Ni-, Pd- and Pt-doped Cu(111)

The reaction free energies and activation barriers for the optimal CO_2 reduction pathways into CH_4 and CH_3OH production are listed in Tables 1 and 2 on the pure and transition metal Ni-, Pd- and Pt-doped Cu(111) surfaces.

Based on the data in Tables 1 and 2, potential energy diagrams for formation of CH_4 and CH_3OH through CO_2 reduction on the pure and transition metal Ni-, Pd- and Pt-doped Cu(111) surfaces are given in Fig. 2–5, respectively. We observed that the activation barriers of CO formation through
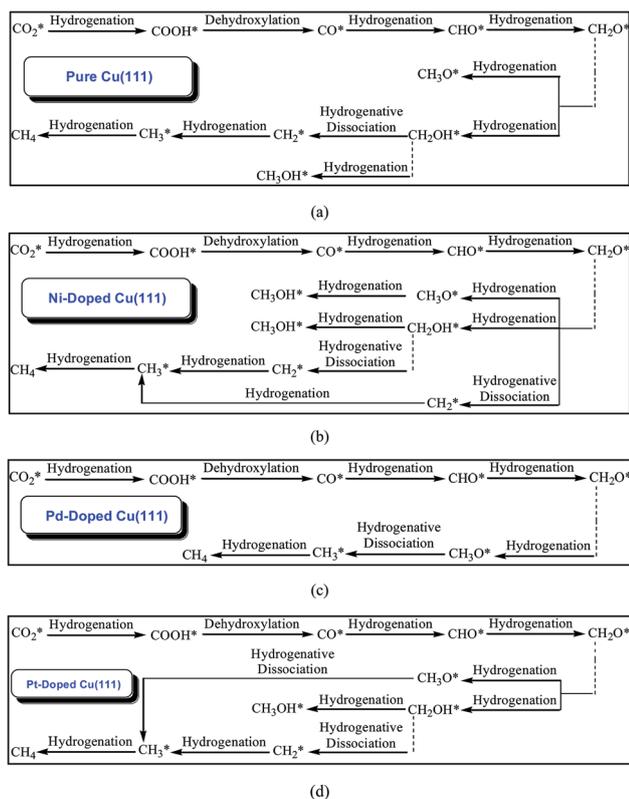
initial CO_2 reduction are considerably decreased by the doping of Ni, Pd and Pt, which is the rate-determining step of CO_2 reduction on the pure Cu(111) surface (ca. 1.18 eV). Thus, the doping of Ni, Pd and Pt can activate CO_2 and enhance the surface activity of Cu catalysts for CO_2 reduction. Therefore, CO formation requires significantly lower activation barriers on Ni and Pt-doped Cu(111) surfaces (ca. 0.40 and 0.65 eV), whereas an activation barrier of 0.83 V is required after doping of Pd (see Fig. S1, S19 and S16†), which may be attributed to chemisorbed CO_2 molecule being observed after doping of Ni and Pt by binding C atom at Ni and Pt sites, whereas only physisorbed

Table 1 The optimal CO_2 reduction pathways into hydrocarbons CH_4 and CH_3OH and the reaction free energies (E_{reac}) and activation barriers (E_{act}) for each elementary step on the pure and Ni-doped Cu(111) surfaces[a]

Reaction paths	Pure Cu(111)		Ni-doped Cu(111)	
	ΔG_{reac} (eV)	E_{act} (eV)	ΔG_{reac} (eV)	E_{act} (eV)
$CO_2(g) + H^* \rightarrow (CO + OH)^*$	0.27	1.18	−0.23	0.40
$(CO + H)^* \rightarrow CHO^*$	0.90	1.06	1.03	1.08
$(CHO + H)^* \rightarrow CH_2O^*$	−0.20	0.72	−0.04	0.28
$(CH_2O + H)^* \rightarrow (CH_2 + OH)^*$	0.01	1.12	0.06	0.24
$(CH_2O + H)^* \rightarrow CH_2OH^*$	0.13	0.95	−0.60	0.27
$(CH_2O + H)^* \rightarrow CH_3O^*$	−1.05	1.86	−0.08	0.24
$(CH_2OH + H)^* \rightarrow CH_2^* + H_2O (l)$	−0.19	0.66	−0.13	0.58
$(CH_2OH + H)^* \rightarrow CH_3OH (l)$	−0.95	0.68	−0.61	0.16
$(CH_2 + H)^* \rightarrow CH_3^*$	−0.83	0.63	−0.55	0.30
$(CH_3 + H)^* \rightarrow CH_4^*$	−0.80	1.03	−0.59	0.21

[a] The asterisk (*) indicates that the species is adsorbed on the surface. The zero point energies (ZPE) for all species, which are obtained by the present DFT calculations, are included in the reaction free energy. For instance, for the reaction step of $(CO + H)^* \rightarrow CHO^*$, the reaction free energy is calculated according to "$E(CHO^*) − E(CO + H)^* + ZPE(CHO^*) − ZPE(CO^*) − ZPE(H^*)$".

Table 2 The optimal CO_2 reduction pathways into hydrocarbons CH_4 and CH_3OH and the reaction energies (E_{reac}) and activation barriers (E_{act}) for each elementary step on Pd- and Pt-doped Cu(111) surfaces

Reaction paths	Pd-doped Cu(111)		Pt-doped Cu(111)	
	ΔG_{reac} (eV)	E_{act} (eV)	E_{reac} (eV)	ΔG_{reac} (eV)
$CO_2(g) + H^* \rightarrow (CO + OH)^*$	0.31	0.83	0.07	0.65
$(CO + H)^* \rightarrow CHO^*$	0.51	0.87	0.41	0.84
$(CHO + H)^* \rightarrow CH_2O^*$	−0.25	0.10	−0.02	0.35
$(CH_2O + H)^* \rightarrow (CH_2 + OH)^*$	0.24	0.52	0.26	0.82
$(CH_2O + H)^* \rightarrow CH_2OH^*$	−0.12	0.68	−0.35	0.59
$(CH_2O + H)^* \rightarrow CH_3O^*$	−0.80	0.06	−0.62	0.17
$(CH_2OH + H)^* \rightarrow CH_2^* + H_2O (l)$	−0.01	0.33	0.10	0.60
$(CH_2OH + H)^* \rightarrow CH_3OH (l)$	−0.86	0.30	−0.53	0.34
$(CH_3O + H)^* \rightarrow CH_3OH (l)$	−0.10	1.86	−0.17	1.36
$(CH_3O + H)^* \rightarrow (CH_3 + OH)^*$	0.01	0.29	−0.12	0.63
$(CH_2 + H)^* \rightarrow CH_3^*$	−0.83	0.35	−0.95	0.33
$(CH_3 + H)^* \rightarrow CH_4^*$	−1.01	0.23	−0.82	0.70

Fig. 1 The optimal reaction pathways of CO_2 reduction into CH_4 and CH_3OH on: (a) pure Cu(111); (b) Ni-doped Cu(111); (c) Pd-doped Cu(111); and (d) Pt-doped Cu(111).
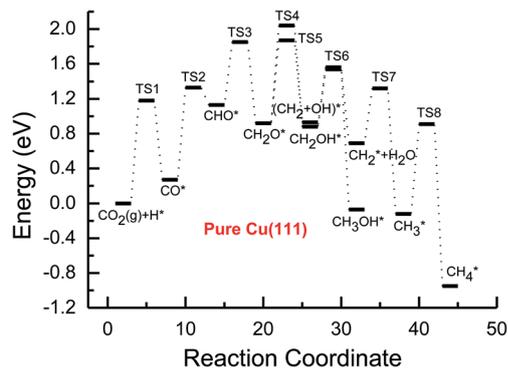
Fig. 2 Potential energy diagrams for the CH_4 and CH_3OH formation through CO_2 reduction on the pure Cu(111) surface. TS stands for transition state.
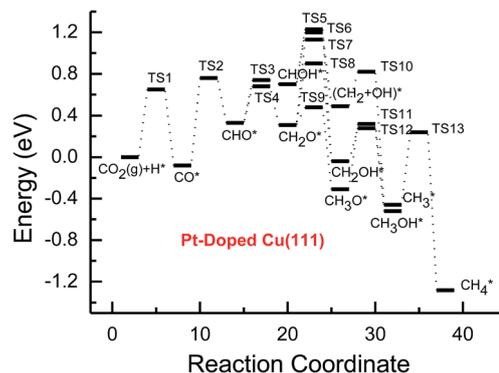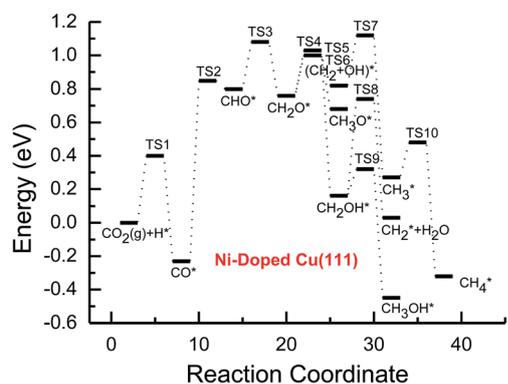

Fig. 3 Potential energy diagrams for CH_4 and CH_3OH formation through CO_2 reduction on the transition metal Ni-doped Cu(111) surface.

Fig. 4 Potential energy diagrams for CH_4 and CH_3OH formation through CO_2 reduction on the transition metal Pd-doped Cu(111) surface.

Fig. 5 Potential energy diagrams for CH_4 and CH_3OH formation through CO_2 reduction on the transition metal Pt-doped Cu(111) surface.
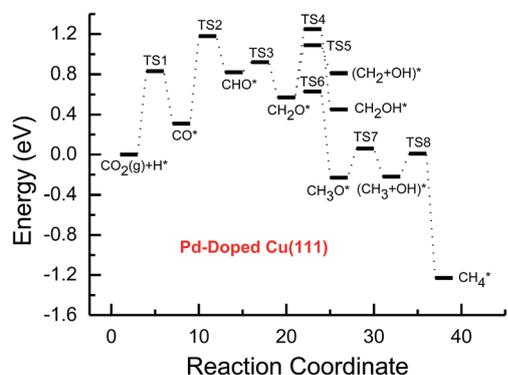
undergo further hydrogenation into CHO, which is in favor of dissociation back to CO and H. For example, CO hydrogenation to form CHO needs to overcome an activation barrier of 1.06 eV on the pure Cu(111) surface, whereas the inverse process only requires an activation barrier of 0.16 eV. The corresponding pathway has nearly equal activation barriers on the Ni-doped Cu(111) surface and the pure Cu(111) surface (1.06 eV *vs.* 1.08 eV), and a very low activation barrier for CHO dissociation back to CO was required (*ca.* 0.10 eV). Both steps may hinder CH_4 and CH_3OH formation in CO_2 reduction on the pure and Ni-doped Cu(111) surfaces. In fact, a large amount of CO was observed experimentally on Cu for CH_3OH synthesis.[67] Based on our present calculations, the doping of Pd and Pt helps to improve the corresponding hydrogenation process. The activation barriers are 0.87 and 0.84 eV for CO hydrogenation after the doping of Pd and Pt, which are 0.19 and 0.22 eV lower than the corresponding barrier on the pure Cu(111) surface, respectively. Moreover, the activation barriers for CHO dissociation back to CO are increased on Pd- and Pt-doped Cu(111) surfaces (see Fig. S11 and S18†), which are 0.10 and 0.27 eV higher than the corresponding barriers on the pure Cu(111) surface, respectively. Improvement of further CO reduction may be attributed to the stronger CO adsorption. The adsorption energy of CO is 0.13 and 0.48 eV stronger after doping of Pd and Pt than that on the pure Cu(111) surface, respectively, *i.e.* the CO intermediate can be stabilized. Our present studies also show that the CO molecule can be stabilized by the doping of Ni. However, CO adsorption is stronger than that on the pure Cu(111) surface by 0.80 eV after doping of Ni, which is significantly higher than that on the Pd- and Pt-doped Cu(111) surfaces, thereby leading to a relatively poor improvement for further CO reduction into CHO. Although the doped Ni atom cannot significantly improve the further CO reduction into CHO, it makes CO formation the most facile to occur. According to our calculations, CO prefers to adsorb on the top sites of Ni, Pd and Pt. In comparison, the energetically most favorable site for CO adsorption is the fcc-hollow site on the pure Cu(111) surface.[63]

Subsequent further CHO reduction into the CH_2O intermediate is the most favorable pathway among various possibilities on the pure and Ni-, Pd- and Pt-doped Cu(111) surfaces (see

CO_2 was observed on the Pd-doped Cu(111) surface. For further CO reduction, CO hydrogenation into CHO was shown to be the preferred reaction pathway on the Ni-, Pd- and Pt-doped Cu(111) surfaces, as obtained on the pure Cu(111) surface.[63] Our previous study and the work from Mei and co-authors[63,66] have shown that CO prefers to desorb from Cu rather than to

Fig. S4, S12 and S19†). The activation barriers of 0.28, 0.10 and 0.35 eV are required for this pathway, respectively, which are significantly lower than that on the pure $Cu(111)$ surface (ca. 0.72 eV). Simultaneously, it can be found that the CHOH intermediate may be formed on the Pt-doped $Cu(111)$ surface since CH_2O and CHOH formation through CHO hydrogenation have nearly equal activation barriers (ca. 0.35 and 0.40 eV). We also observed that the further reduction of CHO is energetically comparable to CHO dissociation back to CO after the doping of Ni, Pd and Pt. Thus, although the doping of Ni has a poor improvement for further CO reduction, it considerably improves the further CHO reduction into key intermediate CH_2O. The significantly lower activation barriers after the doping of Ni, Pd and Pt may be owing to the stronger CHO adsorption. CHO prefers to bind at Ni, Pd and Pt sites through a C atom after the doping of Ni, Pd and Pt, which is 0.67, 0.29 and 0.68 eV more stable than that on the pure $Cu(111)$ surface, respectively. Thus, the CHO intermediate is able to be stabilized and further CHO reduction can be promoted by the doping of Ni, Pd and Pt atoms.

On the Ni-doped $Cu(111)$ surface, CH_2O hydrogenation into CH_3O and CH_2OH, and hydrogenative dissociation into CH_2 may be parallel pathways since they have very low and almost equal activation barriers. The barriers for the corresponding pathways are 0.24, 0.27 and 0.24 eV, respectively. Only CH_3O formation is the most preferred pathway in further CH_2O reduction on the Pd-doped $Cu(111)$ surface with a very low activation barrier of 0.06 eV, which is a non-activated process, as shown in Fig. S13.† On the Pt-doped $Cu(111)$ surface, CH_3O and CH_2OH formations through CH_2O hydrogenation are the most favorable pathways among four possibilities owing to the relatively lower activation barriers (0.21 and 0.59 eV), as shown in Fig. S20.† However, considerably higher activation barriers are required on the pure $Cu(111)$ surface for further CH_2O reduction compared with that on Ni-, Pd- and Pt-doped $Cu(111)$, and the most favorable reduction pathway is hydrogenation of CH_2O into CH_2OH with an activation barrier of 0.95 eV. The significantly lower barriers may be owing to the doping of Ni, Pd and Pt stabilizing the CH_2O intermediate, which adsorbs on the Ni-, Pd- and Pt-doped $Cu(111)$ surfaces through the C atom directly interacting with Ni, Pd and Pt and O atoms interacting with Cu and transition metal M (M = Ni, Pd and Pt). In comparison, the adsorption of CH_2O intermediate on the Ni-, Pd- and Pt-doped $Cu(111)$ surfaces is 0.55, 0.19 and 0.31 eV more stable than that on pure $Cu(111)$, respectively. On the Pt-doped $Cu(111)$ surface, CH_2 and CH_2OH may be able to be formed through CHOH hydrogenative dissociation and direct hydrogenation owing to almost identical activation barriers (ca. 0.53 and 0.54 eV). However, CHOH dissociation back into CHO only requires a very low activation barrier of ca. 0.04 eV, as shown in Fig. S4 and S19,† which is a non-activated process. Thus, although CHOH can be formed on the Pt-doped $Cu(111)$ surface, its further reduction may not be able to occur.

Further reduction of CH_2OH intermediate into CH_3OH is more favorable to occur with an activation barrier as low as 0.16 eV on the Ni-doped $Cu(111)$ surface, which is significantly more facile in contrast with CH_3O further reduction, as shown

in Fig. S6 and S7.† Thus, CH_3OH can be formed easily by CH_2OH hydrogenation after the doping of Ni atom. CH_3O hydrogenative dissociation into the CH_3 intermediate is the most preferred pathway in further CH_3O reduction on the Pd- and Pt-doped $Cu(111)$ surfaces with relatively lower activation barriers of 0.29 and 0.63 eV, respectively. On the Pt-doped $Cu(111)$ surface, CH_3OH and CH_2 can be also formed easily through hydrogenation and hydrogenative dissociation in further reduction of CH_2OH with relatively lower activation barriers of 0.34 and 0.60 eV, respectively. Thus, the doping of Pt may lead to simultaneous formation of CH_2, CH_3 and CH_3OH, as shown in Fig. S22 and S23.† Our previous studies also suggested that CH_3OH and CH_2 were formed on the pure $Cu(111)$ surface through further reduction of CH_2OH with activation barriers of 0.68 and 0.66 eV, respectively.[63] However, the doping of Ni and Pt leads to a significant decrease of the activation barriers for CH_3OH formation. Thus, further CH_2OH reduction can be improved through the doped Ni and Pt atoms, whereas the doping of Pd promotes CH_3O formation and further reduction, leading to enhanced CH_4 and CH_3OH yields. Further reduction of CH_3O was not considered on the pure $Cu(111)$ surface owing to the significantly higher activation barrier of CH_3O formation. The significant promotion effect on further CH_2OH reduction may be owing to the stronger CH_2OH adsorption after doping of Ni and Pt atoms. The binding of CH_2OH is 0.39 and 0.51 eV more stable than that on the pure $Cu(111)$ surface, and it prefers to bind at the top site of the Ni and Pt atoms by C atom on the Ni- and Pt-doped $Cu(111)$ surfaces. Compared with that on the pure $Cu(111)$ surface, CH_3O on the Ni-doped $Cu(111)$ surface is 0.05 eV more stable. However, CH_3O is 0.09 and 0.25 eV less stable after the doping of Pd and Pt than that on the pure $Cu(111)$ surface, which may explain why the CH_3 intermediate can be formed through hydrogenative dissociation of CH_3O after doping of Pd and Pt.

Based on the above analyses, CH_4 production possibly occurs through serial CH_2 hydrogenation on the Ni- and Pt-doped $Cu(111)$ surfaces or direct CH_3 hydrogenation on the Pd- and Pt-doped $Cu(111)$ surfaces. The activation barriers for CH_2 hydrogenation into CH_3 and CH_3 hydrogenation into CH_4 are 0.30 and 0.21 eV, 0.35 and 0.23 eV, 0.33 and 0.70 eV on Ni, Pd- and Pt-doped $Cu(111)$ surfaces (see Fig. S8, S15 and S24†), respectively, which are notable lower than that for the corresponding pathways on the pure $Cu(111)$ surface (0.63 eV and 1.03 eV, respectively). Based on our present calculations, the doping of Ni and Pt helps to stabilize CH_2 and CH_3 intermediates and enhance the corresponding hydrogenation processes, in which CH_2 and CH_3 are 0.43 and 0.22 eV, 0.18 and 0.23 eV more stable after doping of Ni and Pt, respectively. Although CH_3 is 0.07 eV less stable on the Pd-doped $Cu(111)$ surface, the doping of Pd still can improve further CH_3 reduction into CH_4. This may be attributed to different electronic interactions among Ni and Pd, Ni and Pt, which will be confirmed by subsequent electronic structure analysis. Additionally, OH can be formed during the course of CO_2 reduction into CH_4 and CH_3OH on the pure and Ni-, Pd- and Pt-doped $Cu(111)$ surfaces, which may lead to poisoning of surface active sites. Thus, the OH removal to form H_2O is an important step for CO_2

reduction. The activation barriers for OH removal are 1.09, 0.68, 0.56 and 0.21 eV on pure and Ni-, Pd- and Pt-doped Cu(111) surfaces, respectively, as shown in Fig. 6. We observe that the doping of Ni, Pd and Pt atoms significantly decreases the activation barriers of OH removal, which is 0.41, 0.53 and 0.88 eV lower than the corresponding barrier on pure Cu(111), respectively. Therefore, the reduced value of the activation barrier after the doping of Ni atom is lower than that on the Pd- and Pt-doped Cu(111) surfaces. The significant improvement of OH removal on the Pd- and Pt-doped Cu(111) may be owing to the weaker OH adsorption, in which the adsorption of OH is 0.16 and 0.26 eV less stable than that on the pure Cu(111) surface, respectively, whereas the doping of Ni makes OH adsorption 0.08 eV stronger. Thus, the doping of metals with less affinity toward OH, such as Pd and Pt, improves the OH removal step and proves to be more efficient than pure Cu and high OH affinity metal Ni.

On this basis, the effect of the doped Ni, Pd and Pt atoms on the selectivity of the reaction pathways and reduction production can be revealed. The doped Ni, Pd and Pt atoms changed the rate-determining step of CO_2 reduction, which is $(CO_2 + H)^* \rightarrow (CO + OH)^*$ on the pure Cu(111) surface, whereas it is changed into $(CO + H)^* \rightarrow CHO^*$ after the doping of Ni, Pd and Pt. The activation barriers of rate-determining steps are also
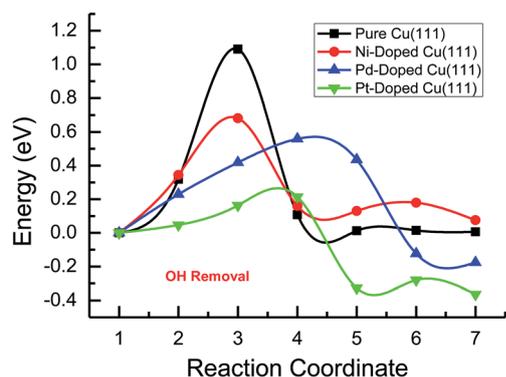
reduced, which are 0.10, 0.31 and 0.34 eV lower than that of the corresponding process on the pure Cu(111) surface, respectively. Simultaneously, we observed that the activation barriers in overall optimal pathways for CO_2 reduction into CH_4 and CH_3OH are 1.88, 1.12, 1.18 and 0.90 eV on the pure and Ni-, Pd- and Pt-doped Cu(111) surfaces, respectively, as shown in Fig. 2–5, in which the barriers are considerably decreased compared with that on pure Cu(111) and the doping of Pt may be able to lead to the strongest catalytic activity owing to the most reduced value. Therefore, higher CH_4 and CH_3OH yields can be expected on the Ni-, Pd- and Pt-doped Cu(111) surfaces. The higher reactivity of Ni-, Pd- and Pt-doped Cu(111) surfaces is also consistent with the previous experimental observations.[36,39–42] The adsorption behavior of intermediates may be able to determine CO_2 reduction activity based on the above discussion. The most stable adsorption sites and adsorption energies for the possible intermediates involved in CO_2 reduction into CH_4 and CH_3OH on the pure and Ni-, Pd- and Pt-doped Cu(111) surfaces are given in Table 3. It is clear that the doping of Ni, Pd and Pt atoms can stabilize the relatively weaker adsorbed C- and O-containing intermediates on the pure Cu(111) surface, such as CO, CHO and CH_2O, where C and O atoms directly interact with the doped Ni, Pd and Pt atoms, thereby resulting in easier formation and reduction of CO, CHO and CH_2O in spite of the doped Ni atom not notably improving further CO reduction into CHO owing to excessively strongly adsorbed CO. However, the stronger adsorbed intermediates, such as CH_3O and OH, are destabilized by the doped Pd and Pt atoms in comparison with pure Cu(111), which make CH_3O formation and further reduction able to occur on the Pd- and Pt-doped Cu(111) surfaces and OH removal be easier. Owing to the high carbon and oxygen affinity of Ni, all intermediates can be stabilized by the doped Ni atom in CO_2 reduction and the Ni-doped Cu(111) surface has the strongest adsorption ability among the Ni-, Pd- and Pt-doped Cu(111) surfaces, whereas the doping of Pd and Pt leads to the weakest and moderate adsorption of most intermediates, respectively, which may explain why Pt-doped Cu(111) surfaces have the best catalytic activity for CO_2 reduction. Thus, it is concluded that moderate adsorbed intermediates on the Cu-based electrocatalyst surfaces will favor CO_2 reduction.

Fig. 6 The minimum energy pathways of OH removal to form H_2O on pure and Ni-, Pd- and Pt-doped Cu(111) surfaces.

Table 3 The most stable adsorption sites and adsorption energies (E_{ads}) for the possible intermediates involved in CO_2 reduction into CH_4 and CH_3OH on pure and Ni-, Pd- and Pt-doped Cu(111) surfaces

Species	Cu(111)		Ni-doped Cu(111)		Pd-doped Cu(111)		Pt-doped Cu(111)	
	Sites	E_{ads} (eV)	Sites	E_{ads} (eV)	Sites	E_{ads} (eV)	Sites	E_{ads} (eV)
COOH	Bridge	−1.56	Bridge	−1.95	Bridge	−1.69	Bridge	−2.03
CO	fcc	−0.80	Top	−1.59	Top	−0.93	Top	−1.28
CHO	fcc	−1.25	Top	−1.93	Top	−1.54	Top	−1.93
CH_2O	fcc	−0.05	fcc	−0.60	fcc	−0.24	fcc	−0.36
CHOH	fcc	−2.50	Top	−3.02	fcc	−2.60	Top	−2.95
CH_2OH	fcc	−0.90	fcc	−1.29	fcc	−1.11	fcc	−1.41
CH_3O	fcc	−2.28	fcc	−2.33	fcc	−2.19	hcp	−2.03
CH_2	fcc	−2.94	fcc	−3.37	fcc	−2.90	fcc	−3.12
CH_3	fcc	−1.36	fcc	−1.58	Top	−1.29	Top	−1.59
OH	fcc	−3.16	fcc	−3.24	hcp	−3.00	hcp	−2.90

3.3 Origin of catalytic activity

3.3.1 The limiting potential and potential-limiting step.

The Ni-, Pd- and Pt-doped Cu(111) surfaces may be able to decrease the overpotentials of CO_2 electroreduction, which can be linked directly to the proton and electron transfer to adsorbed intermediates being strongly bonded to the surface and determines the catalytic activity of the electrocatalysts. Thus, potential dependent reaction free energies and limiting potentials are obtained in order to ascertain the origin of the overpotential and electrocatalytic activity using the computational hydrogen electrode (CHE) model proposed by Nørskov and co-authors.[68] The mechanistic details are elucidated in the ESI.† A thermodynamic equilibrium potential of 0.17 V vs. RHE for hydrocarbons formation is used to calculate the reaction free energies if we assume CO_2 reduction to be in equilibrium and neglect ohmic losses. This model could provide an elegant way to calculate the potential-dependent reaction free energies for each step under electrochemical conditions by avoiding the explicit treatment of solvated protons. The potential where the reaction free energy is zero is referred to as the limiting potential, which serves as an estimate of the onset potential for each intermediate; the most endothermic reaction step in the reaction pathways is referred to as the potential-limiting step.

The calculated limiting potentials (E) and reaction free energies (ΔG_{reac}) at 0.17 V vs. RHE in CO_2 electroreduction to CH_4 and CH_3OH on pure and Ni-, Pd-, and Pt-doped Cu(111) surfaces are listed in Tables 4 and 5. We found that the potential-limiting step is CHO formation (CO* + H$^+$ + e$^-$ → CHO*) with the most positive reaction free energy at 0.17 V vs. RHE on the pure and Ni-, Pd- and Pt-doped Cu(111) surfaces, requiring limiting potentials of −0.60, −0.72, −0.44 and −0.40 V vs. RHE by the CHE model, respectively. It can be observed that the limiting potentials are positively shifted after the doping of Pd and Pt atoms, whereas it is more negative after

Table 4 The limiting potentials (E) and reaction free energies (ΔG_{reac}) at 0.17 V vs. RHE (thermodynamic equilibrium potential) in CO_2 electroreduction to CH_4 and CH_3OH on the pure and Ni-doped Cu(111) surfaces

Possible reduction steps	Pure Cu(111)		Ni-doped Cu(111)	
	E (V)	ΔG_{reac} (eV)	E (V)	ΔG_{reac} (eV)
(a) CO_2* + H$^+$ + e$^-$ → (CO + OH)*	−0.07	0.24	1.11	−0.94
(b) CO* + H$^+$ + e$^-$ → CHO*	−0.60	0.77	−0.72	0.89
(c) CHO* + H$^+$ + e$^-$ → CH_2O*	0.45	−0.28	0.32	−0.15
(d) CH_2O* + H$^+$ + e$^-$ → (CH_2 + OH)*	0.38	−0.21	0.10	0.07
(e) CH_2O* + H$^+$ + e$^-$ → CH_3O*	1.26	−1.09	0.76	−0.59
(f) CH_2O* + H$^+$ + e$^-$ → CH_2OH*	0.23	−0.06	0.07	0.10
(g) CH_2OH* + H$^+$ + e$^-$ → CH_3OH (l)	1.19	−1.02	0.76	−0.59
(h) CH_2OH* + H$^+$ + e$^-$ → CH_2* + H_2O (l)	0.43	−0.26	0.40	−0.23
(i) CH_3O* + H$^+$ + e$^-$ → CH_3OH (l)	0.17	0.00	0.07	0.10
(j) CH_3O* + H$^+$ + e$^-$ → (CH_3 + OH)*	0.24	−0.07	0.22	−0.05
(k) CH_2* + H$^+$ + e$^-$ → CH_3*	1.05	−0.88	0.84	−0.67
(m) CH_3* + H$^+$ + e$^-$ → CH_4*	1.07	−0.90	0.86	−0.69
(n) OH* + H$^+$ + e$^-$ → H_2O (l)	0.12	0.05	0.18	−0.01

Table 5 The limiting potentials (E) and reaction free energies (ΔG_{reac}) at 0.17 V vs. RHE (thermodynamic equilibrium potential) in CO_2 electroreduction to CH_4 and CH_3OH on the Pd- and Pt-doped Cu(111) surfaces

Possible reduction steps	Pd-doped Cu(111)		Pt-doped Cu(111)	
	E (V)	ΔG_{reac} (eV)	E (V)	ΔG_{reac} (eV)
(a) CO_2* + H$^+$ + e$^-$ → (CO + OH)*	−0.11	0.28	0.82	−0.65
(b) CO* + H$^+$ + e$^-$ → CHO*	−0.44	0.61	−0.40	0.57
(c) CHO* + H$^+$ + e$^-$ → CH_2O*	0.35	−0.18	0.08	0.09
(d) CH_2O* + H$^+$ + e$^-$ → (CH_2 + OH)*	−0.08	0.25	−0.16	0.33
(e) CH_2O* + H$^+$ + e$^-$ → CH_3O*	0.97	−0.80	0.69	−0.52
(f) CH_2O* + H$^+$ + e$^-$ → CH_2OH*	0.25	−0.08	0.43	−0.26
(g) CH_2OH* + H$^+$ + e$^-$ → CH_3OH (l)	0.93	−0.76	0.62	−0.45
(h) CH_2OH* + H$^+$ + e$^-$ → CH_2* + H_2O (l)	0.11	0.06	0.00	0.17
(i) CH_3O* + H$^+$ + e$^-$ → CH_3OH (l)	0.21	−0.04	0.36	−0.19
(j) CH_3O* + H$^+$ + e$^-$ → (CH_3 + OH)*	0.01	0.16	0.32	−0.15
(k) CH_2* + H$^+$ + e$^-$ → CH_3*	1.03	−0.86	1.11	−0.94
(m) CH_3* + H$^+$ + e$^-$ → CH_4*	1.14	−0.97	0.84	−0.67
(n) OH* + H$^+$ + e$^-$ → H_2O (l)	0.36	−0.19	0.48	−0.31

the doping of Ni atom, implying that the doped Pd and Pt atoms can decrease the overpotential of this pathway. The strongest CO adsorption on the Ni-doped Cu(111) surface may induce the protonation to be potentially limited, resulting in a relatively high overpotential for CHO formation. The formation of CHO is also the rate-determining step in CO_2 reduction on the Ni-, Pd- and Pt-doped Cu(111) surfaces based on the above kinetic analyses, and its activation barriers are lower after the doping of Pd and Pt atoms, and slightly higher after the doping of Ni atom, compared with that on the pure Cu(111) surface. Although the doped Ni atom leads to more negative limiting potential (−0.72 V) and more positive reaction free energy (0.89 eV) for CHO formation, it can notably shift the limiting potential and reaction free energy to more positive (1.11 V) and more negative values (−0.94 eV) for CO formation (CO_2* + H$^+$ + e$^-$ → (CO + OH)*), respectively, in which the formation of CO has a slightly negative limiting potential of −0.07 V and a positive reaction free energy of 0.24 eV on the pure Cu(111) surface. The above kinetic studies also show that the activation barrier of CO formation is significantly decreased by the doping of Ni atom. Thus, the decreased overpotential for CO formation can be concluded after the doping of Ni. As shown in Table 5, the doping of Pt atom also can significantly shift the limiting potential of CO formation to a more positive value and make the reaction free energy more negative, thus leading to decrease of the overpotential. However, the limiting potential and reaction free energy of CO formation after the doping of Pd are almost unchanged compared with that on the pure Cu(111) surface. These may be owing to chemisorbed CO_2 being observed on Ni- and Pt-doped Cu(111) surfaces and only physisorbed CO_2 is formed on the Pd-doped Cu(111) surface. Simultaneously, the limiting potentials of OH removal are also shifted positively after the doping of Ni, Pd and Pt, which are 0.06, 0.24 and 0.36 V more positive than that on the pure Cu(111) surface, respectively, leading to the reduction of the overpotential. Therefore,

the Pt-doped Cu(111) surface with the weakest OH adsorption has the most positive limiting potential and the most negative reaction free energy, which is in agreement with the above kinetic analyses, suggesting that the doped metals with less affinity toward OH could decrease surface OH poisoning and enhance the catalytic activity. Thus, the best electrocatalytic activity of the Pt-doped Cu(111) surface for CO_2 reduction may be able to be attributed to the simultaneous reduction of over-potential for CO formation and further reduction, and the easiest OH removal.

3.3.2 The analysis of electronic structure. The adsorption behavior and reduction mechanism may be able to be determined by electronic interactions between the Cu(111) surface and the doped transition metals M (M = Ni, Pd and Pt). The analyses of electronic structures facilitate the understanding the origin of catalytic activity of the transition metal Ni-, Pd- and Pt-doped Cu(111) surfaces toward CO_2 reduction. Thus, in order to determine the origin of the catalytic activity and understand the electron transfer between the transition metal M (M = Ni, Pd and Pt) and the Cu(111) surface, we performed local density of states (LDOS) analysis of pure and Ni-, Pd- and Pt-doped Cu(111) surfaces in the present study since it can describe the number of electron at Fermi energy level that are available to be occupied. A high LDOS at the Fermi energy level means that there are many electrons available for occupation. Fig. 7 and 8 give the LDOS of the pure and Ni-, Pd- and Pt-doped Cu(111) surfaces. For comparison, the LDOS of pure Ni, Pd and Pt are

also included. The results show that the doping of Ni, Pd and Pt leads to an obvious change of the s state of Cu at the Fermi energy level compared with that of the pure Cu(111) surface, in which s orbitals of Cu in Ni- and Pt-doped Cu(111) have relatively lower LDOS, as shown in Fig. 7(a), implying that more electrons in the s states of Cu are transferred after the doping of Ni and Pt. The LDOS of the d orbital of Cu in the pure and Ni-, Pd- and Pt-doped Cu(111) are almost unchanged, as shown in Fig. 7(b), suggesting that electron transfer may not occur in the d state of Cu. Thus, the observed significantly lower LDOS of the s states of Cu in Ni- and Pt-doped Cu(111) means that more electrons are transferred, thereby leading to stronger adsorption of reaction intermediates in CO_2 reduction on Ni- and Pt-doped Cu(111) surfaces than that on the Pd-doped Cu(111) surface (Table 3).

In the mean time, we also observed that the s and d states of Ni, Pd and Pt in Ni-, Pd- and Pt-doped Cu(111) are changed significantly near the Fermi energy level compared with those of pure Ni, Pd and Pt, as shown in Fig. 8(a) and (b). The considerably higher LDOS near the Fermi energy level shows that electrons in the s state of Cu are transferred into the s and d states of Ni, Pd and Pt. The highest LDOS in the d states of Ni in Ni-doped Cu(111) may imply that the most electron transfer and strongest interactions occur between Cu and Ni. Thus, the present studies explain why the reaction intermediates have the strongest adsorption on the Ni-doped Cu(111) surface. The relatively weaker interaction between Cu and transition metals Pd and Pt may result in weaker adsorption of intermediates.
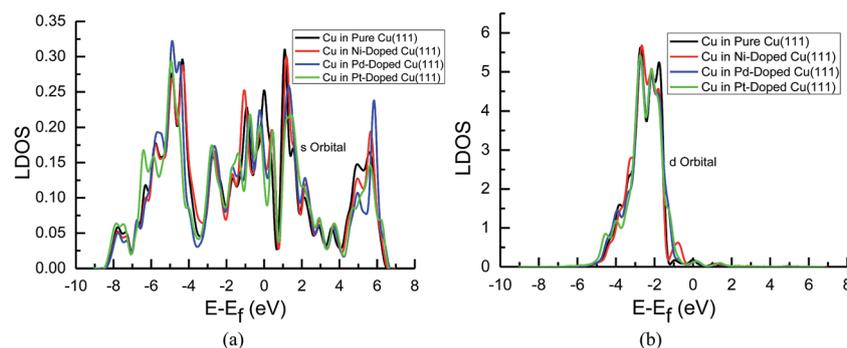

Fig. 7 Local density of states of pure and transition metals Ni-, Pd- and Pt-doped Cu(111) surfaces: (a) s orbital of Cu and (b) d orbital of Cu.
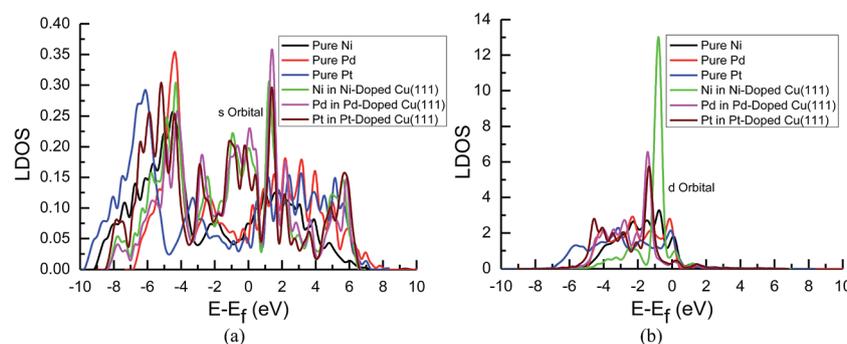

Fig. 8 Local density of states of pure and transition metals Ni-, Pd- and Pt-doped Cu(111) surfaces: (a) s orbitals of Ni, Pd and Pt; and (b) d orbitals of Ni, Pd and Pt.

The d-band center of surface atoms, ε_d, is a key parameter that influences surface adsorption characteristics,[69,70] and its upshift and downshift can be used to judge the catalytic activity of the electrocatalysts.[71–73] The shift of the d-band center into a lower energy level (downshift) corresponds to the weaker adsorption of reaction intermediates, whereas the shift into a higher energy level (upshift) corresponds to the stronger adsorption. Thus, the d-band centers of surface atoms were calculated in pure and Ni-, Pd- and Pt-doped Cu(111), which is the first moment of the projected d-band density of states on the surface atoms referenced to the Fermi energy level. The corresponding values for surface atoms are listed in Table 6. It was found that there is a slight and considerably upshift of the d-band center of surface Cu and Ni atoms (ca. 0.02 and 0.74 eV) in Ni-doped Cu(111) compared with that of the pure metal surfaces, respectively, whereas that of surface Cu atoms is not changed after the doping of Pd and Pt atoms. The relatively lower upshift of the d-band center of the surface Pt atom in Pt-doped Cu(111) is also observed (ca. 0.20 eV). However, the d-band center of the surface Pd atom is downshifted significantly in Pd-doped Cu(111) (ca. −0.34 eV) compared with that of pure Pd. Thus, we conclude that the doping of Ni and Pd can lead to the strongest and weakest adsorption of reaction intermediates on the Ni and Pd-doped Cu(111) surfaces, respectively. Furthermore, the significant upshift of the d-band center of the surface Ni atom and the strongest interaction between CO and the Ni-doped Cu(111) surface may also be able to explain why further CO reduction has the most positive activation barrier and the most negative limiting potential on the Ni-doped Cu(111) surface among the Ni-, Pd- and Pt-doped Cu(111) surfaces, whereas the significant downshift of the d-band center of the surface Pd atom in Pd-doped Cu(111) explains why only physisorbed CO_2 is observed, which even leads to slightly more negative limiting potential for CO formation in comparison with that on pure Cu(111). Accordingly, we infer that the dopant Pt with moderate upshift of the d-band center is the most capable of enhancing the electrocatalytic activity of Cu catalysts for CO_2 reduction, which confirms the above thermodynamic and kinetic studies.

Based on our present calculations, CO formation and further reduction are key reaction steps during the course of CO_2 reduction into hydrocarbons. CO_2 reduction on the Cu catalyst can be promoted and higher hydrocarbons yield may be able to be expected by the doping of transition metals. On the basis of the above discussion, two possible descriptors can be proposed in order to scale the electrocatalytic activity of Cu-based alloy catalysts for CO_2 reduction. One is activation barriers of CO formation and further reduction. The transition metal-doped Cu-based alloy electrocatalysts with lower activation barriers for CO formation and further reduction will exhibit better catalytic activity for CO_2 reduction. For example, the barriers of CO formation are decreased by the doped Ni, Pd and Pt atoms, and those of further CO reduction on the Pd- and Pt-doped Cu(111) surfaces are also reduced. The chemisorbed CO_2 on Cu-based electrocatalyst surfaces will favor the formation of the key intermediate CO, i.e. the doping of Ni and Pt lead to the formation of chemisorbed CO_2 and make CO formation easier. The moderately adsorbed CO on Cu-based electrocatalyst surfaces can avoid CO desorption and poisoning on surface active sites, thereby being in favor of further CO reduction, i.e. the Ni-doped Cu(111) surface has excessively strong CO adsorption, resulting in the highest barrier and the most negative limiting potential for further CO reduction among pure, Ni-, Pd- and Pt-doped Cu(111) surfaces. Another is the electronic structure of the transition metals-doped Cu-based electrocatalysts. The moderate interactions between Cu and transition metals and the moderate upshift of the d-band center of the doped transition metals in transition metal-doped Cu(111) will favor CO_2 reduction, which can lead to moderate adsorption of intermediates. For example, the Ni-doped Cu(111) surface with the strongest interaction between Cu and Ni and the most upshift of the d-band center of the Ni atom, and Pd-doped Cu(111) surface with the downshift of the d-band center of Pd atom have relatively poorer electrocatalytic activity for CO_2 reduction than the Pt-doped Cu(111) surface. Thus, an ideal Cu-based alloy electrocatalyst toward CO_2 reduction should be able reduce activation barriers for CO formation and further reduction, and should have moderate electron interactions between Cu and the doped transition metals, and a moderate upshift of the d-band center of the doped transition metals. In these ways, CO_2 reduction pathways can be facilitated and the yield of hydrocarbons CH_4 and CH_3OH can be enhanced.

4. Conclusions

In our present paper, the effect of the doped transition metal M (M = Ni, Pd and Pt) on CO_2 reduction pathways and the origin of the electrocatalytic activity are investigated systematically by focusing on the CH_4 and CH_3OH formation pathways based on DFT calculations of the key adsorbates associated with the computational hydrogen electrode model. Our studies show that the doping of Ni, Pd and Pt can promote CO_2 reduction and influence the selectivity of the reduction pathways and products, in which the doping of Pt may be able to lead to the strongest catalytic activity. The adsorption behavior of intermediates may be able to determine the CO_2 reduction activity. The destabilization of the stronger adsorbed intermediates to

Table 6 The DFT calculated d-band center, ε_d of surface atoms in pure and Ni-, Pd- and Pt-doped Cu(111)

Surface atoms		ε_d (eV)	$\Delta\varepsilon_d{}^a$ (eV)
Pure Cu		−2.52	—
Pure Ni		−1.79	—
Pure Pd		−2.02	—
Pure Pt		−2.69	—
Ni-doped Cu(111)	Cu	−2.50	0.02
	Ni	−1.05	0.74
Pd-doped Cu(111)	Cu	−2.52	0.00
	Pd	−2.36	−0.34
Pt-doped Cu(111)	Cu	−2.52	0.00
	Pt	−2.49	0.20

^{a} $\Delta\varepsilon_d$ represents difference of the d-band center, ε_d of surface atoms between surface atoms in Ni-, Pd- and Pt-doped Cu(111) and pure surface atoms.

CH_3O by the doped Pd and Pt atoms make CH_3O formation and further reduction occur, thus the selectivity of reduction pathways is revealed. Owing to high carbon and oxygen affinity of Ni, all intermediates can be stabilized by the doped Ni atom. The Ni-doped Cu(111) surface has the strongest adsorption ability among the Ni-, Pd- and Pt-doped Cu(111) surfaces, whereas the doping of Pd and Pt leads to the weakest and moderate adsorption of most intermediates, respectively, which may explain why Pt-doped Cu(111) surfaces have the best catalytic activity for CO_2 reduction. Thus, it is concluded that moderate adsorbed intermediates on the Cu-based electrocatalyst surfaces will favor CO_2 reduction.

The enhanced electrocatalytic activity of the transition metal-doped Cu(111) surfaces may be owing to the decrease of the overpotential and electronic interactions between Cu and the transition metals. Further reduction of CO into CHO is the potential-limiting step on the pure and Ni-, Pd- and Pt-doped Cu(111) surfaces. The doping of Pd and Pt atoms can reduce the overpotential of CHO formation, whereas the doped Ni makes it slightly higher in comparison with pure Cu(111). The overpotential of CO formation is notably decreased after the doping of Ni, which is the rate-determining step on pure Cu(111). The significantly reduced overpotential for CO formation is also observed on the Pt-doped Cu(111). However, a slightly increased overpotential is obtained on the Pd-doped Cu(111) for CO formation. Simultaneously, the Pt-doped Cu(111) surface has the lowest overpotential for OH removal, suggesting that the doped metals with less affinity toward OH could enhance the catalytic activity. Thus, the doped Pt can simultaneously reduce the overpotential for CO formation and further reduction and most easily remove OH. The electronic structures analyses show that there is a moderate interaction between Cu and Pt and a moderate upshift of the d-band center of Pt. These analyses confirm why the Pt-doped Cu(111) surface has the best electrocatalytic activity for CO_2 reduction.

Two possible descriptors can be proposed in order to scale the electrocatalytic activity of Cu-based electrocatalysts for CO_2 reduction. One is activation barriers of CO formation and further reduction. The transition metal-doped Cu-based electrocatalysts with lower barriers will exhibit better catalytic activity for CO_2 reduction. The chemisorbed CO_2 on the Cu-based electrocatalyst will favor the formation of the key intermediate CO. The moderate adsorbed CO on the Cu-based electrocatalyst can avoid CO desorption and poisoning on surface active sites, thereby being in favor of further reduction of CO. Another is the electronic structure of the Cu-based electrocatalysts. The moderate interactions between Cu and the doped transition metals and the moderate upshift of the d-band center of the doped transition metals will be in favor of CO_2 reduction. Thus, an ideal Cu-based electrocatalyst should be able to reduce barriers for CO formation and further reduction, and should have moderate interactions between Cu and the doped transition metals, and a moderate upshift of d-band center of the doped transition metals. In these ways, CO_2 reduction pathways can be facilitated and the yield of hydrocarbons CH_4 and CH_3OH can be enhanced.

References

1 A. Goeppert, M. Czaun, R. B. May, G. K. S. Prakash, G. A. Olah and S. R. Narayanan, Carbon Dioxide Capture from the Air Using a Polyamine Based Regenerable Solid Adsorbent, *J. Am. Chem. Soc.*, 2011, **133**, 20164–20167.

2 C. Graves, S. D. Ebbesen, M. Mogensen and K. S. Lackner, Sustainable Hydrocarbon Fuels by Recycling CO_2 and H_2O with Renewable or Nuclear Energy, *Renewable Sustainable Energy Rev.*, 2011, **15**, 1–23.

3 D. T. Whipple and P. J. A. Kenis, Prospects of CO_2 Utilization *via* Direct Heterogeneous Electrochemical Reduction, *J. Phys. Chem. Lett.*, 2011, **1**, 3451–3458.

4 W. L. Zhu, R. Michalsky, O. Metin, H. F. Lv, S. J. Guo, C. J. Wright, X. L. Sun, A. A. Peterson and S. H. Sun, Monodisperse Au Nanoparticles for Selective Electrocatalytic Reduction of CO_2 to CO, *J. Am. Chem. Soc.*, 2013, **135**, 16833–16836.

5 K. P. Kuhl, E. R. Cave, D. N. Abram and T. F. Jaramillo, New Insights into the Electrochemical Reduction of Carbon Dioxide on Metallic Copper Surfaces, *Energy Environ. Sci.*, 2012, **5**, 7050–7059.

6 K. J. P. Schouten, E. Pérez Gallent and M. T. M. Koper, Structure Sensitivity of the Electrochemical Reduction of Carbon Monoxide on Copper Single Crystals, *ACS Catal.*, 2013, **3**, 1292–1295.

7 M. Le, M. Ren, Z. Zhang, P. T. Sprunger, R. L. Kurtz and J. C. Flake, Electrochemical Reduction of CO_2 to CH_3OH at Copper Oxide Surfaces, *J. Electrochem. Soc.*, 2011, **158**, E45–E49.

8 X. Nie, G. L. Griffin, M. J. Janik and A. Asthagiri, Surface Phases of Cu_2O(111) under CO_2 Electrochemical Reduction Conditions, *Catal. Commun.*, 2014, **52**, 88–91.

9 C. W. Li and M. W. Kanan, CO_2 Reduction at Low Overpotential on Cu Electrodes Resulting from the Reduction of Thick Cu_2O Films, *J. Am. Chem. Soc.*, 2012, **134**, 7231–7234.

10 B. Innocent, D. Liaigre, D. Pasquier, F. Ropital, J. M. Legerand and K. B. Kokoh, Electro-Reduction of Carbon Dioxide to Formate on Lead Electrode in Aqueous Medium, *J. Appl. Electrochem.*, 2009, **39**, 227–232.

11 Y. Chen and M. W. Kanan, Tin Oxide Dependence of the CO_2 Reduction Efficiency on Tin Electrodes and Enhanced

Activity for Tin/Tin Oxide Thin-Film Catalysts, *J. Am. Chem. Soc.*, 2012, **134**, 1986–1989.

12 M. Jitaru, D. A. Lowy, M. Toma, B. C. Toma and L. Oniciu, Electrochemical Reduction of Carbon Dioxide on Flat Metallic Cathodes, *J. Appl. Electrochem.*, 1997, **27**, 875–889.

13 H. Noda, S. Ikeda, Y. Oda, K. Imai, M. Maeda and K. Ito, Electrochemical Reduction of Carbon Dioxide at Various Metal Electrodes in Aqueous Potassium Hydrogen Carbonate Solution, *Bull. Chem. Soc. Jpn.*, 1990, **63**, 2459–2462.

14 A. A. Peterson and J. K. Nørskov, Activity Descriptors for CO_2 Electroreduction to Methane on Transition-Metal Catalysts, *J. Phys. Chem. Lett.*, 2012, **3**, 251–258.

15 K. P. Kuhl, T. Hatsukade, E. R. Cave, D. N. Abram, J. Kibsgaard and T. F. Jaramillo, Electrocatalytic Conversion of Carbon Dioxide to Methane and Methanol on Transition Metal Surfaces, *J. Am. Chem. Soc.*, 2014, **136**, 14107–14113.

16 B. A. Rosen, A. Salehi-Khojin, M. R. Thorson, W. Zhu, D. T. Whipple, P. J. A. Kenis and R. I. Masel, Ionic Liquid-Mediated Selective Conversion of CO_2 to CO at Low Overpotentials, *Science*, 2011, **334**, 643–644.

17 J. F. Hull, Y. Himeda, W. H. Wang, B. Hashiguchi, R. Periana, D. J. Szalda, J. T. Muckerman and E. Fujita, Reversible Hydrogen Storage Using CO_2 and a Proton-Switchable Iridium Catalyst in Aqueous Media under Mild Temperatures and Pressures, *Nat. Chem.*, 2012, **4**, 383–388.

18 R. Angamuthu, P. Byers, M. Lutz, A. L. Spek and E. Bouwman, Electrocatalytic CO_2 Conversion to Oxalate by a Copper Complex, *Science*, 2010, **327**, 313–315.

19 V. Tripkovic, M. Vanin, M. Karamad, M. E. Björketun, K. W. Jacobsen, K. S. Thygesen and J. Rossmeisl, Electrochemical CO_2 and CO Reduction on Metal-Functionalized Porphyrin-Like Graphene, *J. Phys. Chem. C*, 2013, **117**, 9187–9195.

20 Y. Hori, Electrochemical CO_2 Reduction on Metal Electrodes, in *Modern Aspects of Electrochemistry*, ed. G. Constantinos, C. Vayenas, R. E. White and M. E. Gamboa-Aldeco, Springer, New York, 2008, vol. 42, pp. 89–189.

21 N. Yang, F. Gao and C. E. Nebel, Diamond Decorated with Copper Nanoparticles for Electrochemical; Reduction of Carbon Dioxide, *Anal. Chem.*, 2013, **85**, 5764–5769.

22 W. Tang, A. A. Peterson, A. S. Varela, Z. P. Jovanov, L. Bech, W. J. Durand, S. Dahl, J. K. Nørskov and I. Chorkendorff, The Importance of Surface Morphology in Controlling the Selectivity of Polycrystalline Copper for CO_2 Electroreduction, *Phys. Chem. Chem. Phys.*, 2012, **14**, 76–81.

23 Y. Hori, K. Kikuchi, A. Murata and S. Suzuki, Production of Methane and Ethylene in Electrochemical Reduction of Carbon Dioxide at Copper Electrode in Aqueous Hydrogen Carbonate Solution, *Chem. Lett.*, 1986, **15**, 897–898.

24 Y. Hori, A. Murata, R. Takahashi and S. Suzuki, Electroreduction of CO to CH_4 and C_2H_4 at a Copper Electrode in Aqueous Solutions at Ambient Temperature and Pressure, *J. Am. Chem. Soc.*, 1987, **109**, 5022–5023.

25 R. L. Cook, R. C. MacDuff and A. F. Sammells, Evidence for Formaldehyde, Formic Acid, and Acetaldehyde as Possible Intermediates during Electrochemical Carbon Dioxide Reduction at Copper, *J. Electrochem. Soc.*, 1989, **136**, 1982–1984.

26 Y. Hori, A. Murata and R. Takahashi, Formation of Hydrocarbons in the Electrochemical Reduction of Carbon Dioxide at a Copper Electrode in Aqueous Solution, *J. Chem. Soc., Faraday Trans. 1*, 1989, **85**, 2309–2326.

27 A. A. Peterson and J. K. Nørskov, Activity Descriptors for CO_2 Electroreduction to Methane on Transition-Metal Catalysts, *J. Phys. Chem. Lett.*, 2012, **3**, 251–258.

28 K. P. Kuhl, E. Cave, D. N. Abram and T. F. Jaramillo, New Insights into the Electrochemical Reduction of Carbon Dioxide on Metallic Copper Surfaces, *Energy Environ. Sci.*, 2012, **5**, 7050–7059.

29 J. G. Chen, C. A. Menning and M. B. Zellner, Monolayer Bimetallic Surfaces: Experimental and Theoretical Studies of Trends in Electronic and Chemical Properties, *Surf. Sci. Rep.*, 2008, **63**, 201–254.

30 W. Yu, M. D. Porosoff and J. G. Chen, Review of Pt-Based Bimetallic Catalysis: From model Surfaces to Supported Catalysts, *Chem. Rev.*, 2012, **112**, 5780–5817.

31 D. A. Hansgen, D. G. Vlachos and J. G. Chen, Using First Principles to Predict Bimetallic Catalysts for the Ammonia Decomposition Reaction, *Nat. Chem.*, 2010, **2**, 484–489.

32 J. K. Nørskov, T. Bligaard, J. Rossmeisl and C. H. Christensen, Towards the Computational Design of Solid Catalysts, *Nat. Chem.*, 2009, **1**, 37–46.

33 N. D. Subramanian, G. Balaji, C. S. S. R. Kumar and J. J. Spivey, Development of Cobalt–Copper Nanoparticles as Catalysts for Higher Alcohol Synthesis from Syngas, *Catal. Today*, 2009, **147**, 100–106.

34 N. Schumacher, K. Andersson, L. C. Grabow, M. Mavrikakis, J. Nerlov and I. Chorkendorff, Interaction of Carbon Dioxide with Cu Overlayers on Pt(111), *Surf. Sci.*, 2008, **602**, 702–711.

35 M. Watanabe, M. Shibata, A. Kato, M. Azuma and T. Sakata, Design of Alloy Electrocatalysts for CO_2 Reduction III. The Selective and Reversible Reduction of CO_2 on Cu Alloy Electrodes, *J. Electrochem. Soc.*, 1991, **138**, 3382–3389.

36 X. Y. Zhao, B. B. Luo, R. Long, C. M. Wang and Y. J. Xiong, Composition-Dependent Activity of Cu-Pt Alloy Nanocubes for Electrocatalytic CO_2 Reduction, *J. Mater. Chem. A*, 2015, **3**, 4134–4138.

37 J. Christophe, T. Doneux and C. Buess-Herman, Electroreduction of Carbon Dioxide on Copper-Based Electrodes: Activity of Copper Single Crystals and Copper–Gold Alloys, *Electrocatalysis*, 2012, **3**, 139–146.

38 Z. Xu, E. Lai, Y. Shao-Horn and K. Hamad-Schifferli, Compositional Dependence of the Stability of AuCu Alloy Nanoparticles, *Chem. Commun.*, 2012, **48**, 5626–5628.

39 J. Nerlov and I. Chorkendorff, Methanol Synthesis from CO_2, CO, and H_2 over Cu(100) and Ni/Cu(100), *J. Catal.*, 1999, **181**, 271–279.

40 J. Nerlov, S. Sckerl, J. Wambach and I. Chorkendorff, Methanol Synthesis from CO_2, CO and H_2 over Cu(100) and Cu(100) Modified by Ni and Co, *Appl. Catal., A*, 2000, **191**, 97–109.

41 E. Vesselli, L. D. Rogatis, X. Ding, A. Baraldi, L. Savio, L. Vattuone, M. Rocca, P. Fornasiero, M. Peressi,

A. Baldereschi, R. Rosei and G. Comelli, Carbon Dioxide Hydrogenation on Ni(110), *J. Am. Chem. Soc.*, 2008, **130**, 11417–11422.

42 X. Liu, L. S. Zhu, H. Wang, G. Y. He and Z. Y. Biao, Catalysis Performance Comparison for Electrochemical Reduction of CO_2 on Pd–Cu/Graphene Catalyst, *RSC Adv.*, 2016, **6**, 38380–38387.

43 P. J. Berlowitz and D. W. Goodman, Kinetics of Methanol and Methane Synthesis over Pd/SiO$_2$ and Pd/La$_2$O$_3$, *J. Catal.*, 1987, **108**, 364–368.

44 M. L. Poutsma, L. F. Elek, P. A. Ibarbia, A. P. Risch and J. A. Rabo, Selective Formation of Methanol from Synthesis Gas over Palladium Catalysts, *J. Catal.*, 1978, **52**, 157–168.

45 Y. A. Ryndin, R. F. Hicks, A. T. Bell and Y. I. Yermakov, Effects of Metal-Support Interactions on the Synthesis of Methanol over Palladium, *J. Catal.*, 1981, **70**, 287–297.

46 J. P. Reilly, D. O'Connell and C. J. Barnes, Modification of Formate Stability by Alloying: the Cu(100)-c(2 × 2)-Pt System, *J. Phys.: Condens. Matter*, 1999, **11**, 8417–8430.

47 Y. X. Yang, M. G. White and P. Liu, Theoretical Study of Methanol Synthesis from CO_2 Hydrogenation on Metal-Doped Cu(111) Surfaces, *J. Phys. Chem. C*, 2012, **116**, 248–256.

48 P. Hirunsit, Electroreduction of Carbon Dioxide to Methane on Copper, Copper–Silver, and Copper–Gold Catalysts: A DFT Study, *J. Phys. Chem. C*, 2013, **117**, 8262–8268.

49 P. Hirunsit, W. Soodsawang and J. Limtrakul, CO_2 Electrochemical Reduction to Methane and Methanol on Copper-Based Alloys: Theoretical Insight, *J. Phys. Chem. C*, 2015, **119**, 8238–8249.

50 M. Qiu, Z. X. Fang, Y. Li, J. Zhu, X. Huang, K. N. Ding and W. K. Chen, First-Principles Investigation of the Activation of CO_2 Molecule on TM/Cu (TM = Fe, Co and Ni) Surface Alloys, *Appl. Surf. Sci.*, 2015, **353**, 902–912.

51 M. Qiu, Y. Liu, J. Wu, Y. Li, X. Huang, W. K. Chen and Y. F. Zhang, Theoretical Investigations of the Activation of CO_2 on the Transition Metal-Doped Cu(100) and Cu(111) Surfaces, *Chin. J. Struct. Chem.*, 2016, **35**, 669–678.

52 S. Baroni, A. Dal Corso, S. de Gironcoli and P. Giannozzi, *PWSCF and PHONON: Plane-Wave Pseudo-Potential Codes*, 2001, http://www.pwscf.org.

53 A. Kokalj, XCrySDen—A New Program for Displaying Crystalline Structures and Electron Densities, *J. Mol. Graphics Modell.*, 1999, **17**, 176–179.

54 A. Kokalj and M. Causà, Scientific Visualization in Computational Quantum Chemistry, in *Proceedings of High Performance Graphics Systems and Applications European Workshop*, CINECA-Interuniversity Consortium, Bologna, Italy, 2000.

55 A. Kokalj and M. Causà, *XCrySDen: (X-Window) CRYstalline Structures and DENsities*, 2001, http://www-k3.ijs.si/kokalj/xc/XCrySDen.html.

56 J. P. Perdew, K. Burke and M. Ernzerhof, Generalized Gradient Approximation Made Simple, *Phys. Rev. Lett.*, 1996, **77**, 3865–3868.

57 D. Vanderbilt, Soft Self-Consistent Pseudopotentials in a Generalized Eigenvalue Formalism, *Phys. Rev. B: Condens. Matter Mater. Phys.*, 1990, **41**, 7892–7895.

58 J. Greeley, A. A. Gokhale, J. Kreuser, J. A. Dumesic, H. Topsøe, N. Y. Topsøe and M. Mavrikakis, CO Vibrational Frequencies on Methanol Synthesis Catalysts: A DFT study, *J. Catal.*, 2003, **213**, 63–72.

59 W. M. Haynes, *CRC Handbook of Chemistry and Physics*, CRC Press/Taylor and Francis, Boca Raton, FL, 93rd edn, Internet Version 2012, 2012.

60 M. Methfessel and A. T. Paxton, High-Precision Sampling for Brillouin-zone Integration in Metals, *Phys. Rev. B: Condens. Matter Mater. Phys.*, 1989, **40**, 3616–3621.

61 B. Hammer and J. K. Nørskov, Theoretical Surface Science and Catalysis-Calculations and Concepts, *Adv. Catal.*, 2000, **45**, 71–129.

62 H. A. Hansen, C. Shi, A. C. Lausche, A. A. Peterson and J. K. Nørskov, Bifunctional Alloys for the Electroreduction of CO_2 and CO, *Phys. Chem. Chem. Phys.*, 2016, **18**, 9194–9201.

63 L. H. Ou, Chemical and Electrochemical Hydrogenation of CO_2 to Hydrocarbons on Cu Single Crystal Surfaces: Insights into the Mechanism and Selectivity from DFT Calculations, *RSC Adv.*, 2015, **5**, 57361–57371.

64 G. Henkelman and H. Jonsson, Improved Tangent Estimate in the Nudged Elastic Band Method for Finding Minimum Energy Paths and Saddle Points, *J. Chem. Phys.*, 2000, **113**, 9978–9985.

65 G. Henkelman, B. P. Uberuaga and H. Jonsson, A Climbing Image Nudged Elastic Band Method for Finding Saddle Points and Minimum Energy Paths, *J. Chem. Phys.*, 2000, **113**, 9901–9904.

66 Y. F. Zhao, Y. Yang, C. Mims, C. H. F. Peden, J. Li and D. Mei, Insight into Methanol Synthesis from CO_2 Hydrogenation on Cu(111): Complex Reaction Network and the Effects of H$_2$O, *J. Catal.*, 2011, **281**, 199–211.

67 Y. X. Yang, J. Evans, J. A. Rodriguez, M. G. White and P. Liu, Fundamental Studies of Methanol Synthesis from CO_2 Hydrogenation on Cu(111), Cu Clusters, and Cu/ZnO(0001), *Phys. Chem. Chem. Phys.*, 2010, **12**, 9909–9917.

68 J. K. Nørskov, J. Rossmeisl, A. Logadottir, L. Lindqvist, J. R. Kitchin, T. Bligaard and H. Jónsson, Origin of Overpotential for Oxygen Reduction at a Fuel-Cell Cathode, *J. Phys. Chem. B*, 2004, **108**, 17886–17892.

69 B. Hammer and J. K. Nørskov, Electronic Factors Determining the Reactivity of Metal Surfaces, *Surf. Sci.*, 1995, **343**, 211–220.

70 B. Hammer and J. K. Nørskov, Why Gold is the Noblest of All the Metals, *Nature*, 1995, **376**, 238–240.

71 J. Greeley, J. K. Nørskov and M. Mavrikakis, Electronic Structure and Catalysis on Metal Surfaces, *Annu. Rev. Phys. Chem.*, 2002, **53**, 319–348.

72 B. Hammer, Y. Morikawa and J. K. Nørskov, CO Chemisorption at Metal Surfaces and Overlayers, *Phys. Rev. Lett.*, 1996, **76**, 2141–2144.

73 M. Gajdoš, A. Eichler and J. Hafner, CO Adsorption on Close-Packed Transition and Noble Metal Surfaces: Trends from *ab initio* Calculations, *J. Phys.: Condens. Matter*, 2004, **16**, 1141–1164.